speed camera capable of recording up to 1000 frames per second. The resulting video is then analyzed to determine the radius r_0 of the bubble, the hole size R at which the ripples are first observed, and the number of ripples n^*. Because the hole expands very fast at first, R is much larger than R_c by the time the bubble begins to collapse. To compare the experiments with the theory, in which R enters as a parameter, we measured the latter at the onset of the instability for each given size of the bubble. The quantitative measurements are compared with the theoretical predictions for the dependence of n^* on the bubble size in Fig. 2. On a more qualitative level, the experiments show a suppression of the instability for small bubbles, in agreement with the threshold conditions above.

We conclude with a discussion of possible refinements of the theory and their relation to the geometric nature of the problem. A more complete theory would incorporate a (flattened) hemisphere as the initial condition, rather than a cone. Also, because of the progressive drainage of the liquid, the thickness t acquires a dependence on r (and time). This in turn implies nonuniform rigidity $K(r)$ and mass $\mu(r)$, leading to functions f, g, φ, ψ, and P of a more complicated form. On a more fundamental level, all these aspects should be addressed in terms of the coupled hydrodynamics of the slow viscous (liquid) flow and the rapid air flow (*13*). Yet the strong geometrical constraints involved in the problem are suggestive of the robustness of the results.

The question we have answered is akin to that of applying a curved surface onto a flat one in the most economical way, a problem that has taxed cartographers for many centuries and lies at the birth of differential geometry. It is also somewhat of an inverse counterpart to the problem of fitting a flat sheet to a three-dimensional landscape, which has been studied in various contexts (*15–17*) and is an issue that still vexes fashion designers. The relevance of the geometrical constraints is manifest, for example, in the strong dependence of the rippling on the size of the opening, which is closely related to a well-known theorem by Gauss (*18*), Jellett (*19*), and others, according to which (loosely put) a closed surface cannot be bent without being stretched, whereas an open surface can be bent inextensionally. Similarly, we find that a smaller hole implies a relatively stiffer bubble and hampers the rippling. Although the precise forms of the functions φ and ψ arise from the physical constraints and dynamics imposed by the forces and various boundary conditions, the essence is in the geometry.

References and Notes

1. G. Debrégeas, P.-G. de Gennes, F. Brochard-Wyart, *Science* **279**, 1704 (1998).
2. D. Brush and B. Almroth, *Buckling of Bars, Plates and Shells* (McGraw-Hill, New York, 1975).
3. G. I. Taylor, in *Proceedings of the 12th International Congress of Applied Mechanics* (Springer-Verlag, New York, 1969), p. 382.
4. L. Mahadevan, W. S. Ryu, A. D. T. Samuel, *Nature* **392**, 140 (1998); *Nature* **403**, 502 (2000).
5. G. Debrégeas, P. Martin, F. Brochard-Wyart, *Phys. Rev. Lett.* **75**, 3886 (1995).
6. Whereas surface tension drives the expansion of the hole, rippling is dominated by gravity and viscosity, and we neglect any surface tension–related considerations in the remainder.
7. For a review of elasticity theory, see L. D. Landau and E. M. Lifshitz, *Theory of Elasticity* (Pergamon, New York, ed. 3, 1986); A. E. H. Love, *A Treatise on the Mathematical Theory of Elasticity* (Dover, New York, ed. 4, 1944).
8. The fact that the unperturbed surface is curved plays an essential role here. For a plane, bending energy dominates in the limit of a small deformation, with respect to stretching. For more details, see (*7*).
9. J. D. Buckmaster, A. Nachman, L. Ting, *J. Fluid Mech.* **69**, 1 (1975).
10. P. D. Howell, *Eur. J. Appl. Math.* **7**, 321 (1996).
11. Exact inextensibility requires that each point on the surface be displaced in the three dimensions in which the cone is imbedded: vertical, radial, and azimuthal. Of course, the three displacements are coupled, but, in the limit $\alpha \ll 1$, the radial and angular components are negligibly smaller (by a factor α) than the vertical deformation (*13*). Also, we note that the form of these "inextensibility conditions" depends on the unperturbed configuration, which, in particular, is curved.
12. Here (for $x \in [1, \infty]$),
$$\varphi(x) = \frac{2(x - 1 - \ln x)}{x^2 - 4x + 3 + 2\ln x} \geq 0$$
$$\psi(x) = \frac{(x-1)^3}{3(x^2 - 4x + 3 + 2\ln x)} \geq 0$$
and $f(x)$, $g(x,y)$ are similar rational functions of x, $\ln x$, and y.
13. For the corresponding calculations, see R. da Silveira, S. Chaïeb, L. Mahadevan, in preparation.
14. As the bubble continues to fall, this time scale may vary and so may the number of ripples. However, this last possibility is unlikely, owing to the large forces required to introduce new ripples or remove existing ones.
15. Y. Kantor, M. Kardar, D. R. Nelson, *Phys. Rev. Lett.* **57**, 791 (1986).
16. A. Lobkovksy, S. Gentges, H. Li, D. Morse, T. Witten, *Science* **270**, 1482 (1995).
17. E. Cerda, S. Chaïeb, F. Melo, L. Mahadevan, *Nature* **401**, 46 (1999).
18. M. Spivak, *A Comprehensive Introduction to Differential Geometry* (Publish or Perish, ed. 2, 1979), vol. 1.
19. J. H. Jellett, *Dublin R. Irish Acad. Trans.* **22** (1855).

20. R.d.S. thanks G. Debrégeas for introducing him to the problem and sharing enthusiasm and insight, and M. Kardar for his guidance and comments. S.C. thanks G. McKinley for his support. Supported by NSF grant DMR-98-05833 (R.d.S.), NASA grant NAG3-2155 (S.C.), and the Karl van Tassel Chair at MIT (L.M.).

24 June 1999; accepted 5 January 2000

Control of Thickness and Orientation of Solution-Grown Silicon Nanowires

Justin D. Holmes,† Keith P. Johnston, R. Christopher Doty, Brian A. Korgel*

Bulk quantities of defect-free silicon (Si) nanowires with nearly uniform diameters ranging from 40 to 50 angstroms were grown to a length of several micrometers with a supercritical fluid solution-phase approach. Alkanethiol-coated gold nanocrystals (25 angstroms in diameter) were used as uniform seeds to direct one-dimensional Si crystallization in a solvent heated and pressurized above its critical point. The orientation of the Si nanowires produced with this method could be controlled with reaction pressure. Visible photoluminescence due to quantum confinement effects was observed, as were discrete optical transitions in the ultraviolet-visible absorbance spectra.

One-dimensional quantum wires are expected to play a vital role as both interconnects and functional components in future mesoscopic electronic and optical devices and also to provide an opportunity to test fundamental quantum mechanical concepts (*1, 2*). As the wire diameter approaches the carrier de Broglie wavelength, quantum confinement effects shift band gap energies and, in Si, induce visible photoluminescence (*3*). The electronic and optical properties of the nanowires strongly depend on size; therefore, size control and tunability are key to the success of any method of synthesizing quantum wires. Dimensionality also affects the material properties of nanowires. The absence of translational symmetry in Si could profoundly affect the electronic properties: Bulk Si is an indirect semiconductor with a band gap of 1.1 eV, whereas linear polysilane chains exhibit a 3.89-eV direct gap (*4*). The lattice orientation in a wire can provide a tuning parameter, unavailable in quantum dots, to adjust material properties to suit particular applications. In carbon nanotubes, for example, the bonding geometry and orientation profoundly affect the electronic structure and can lead to either metallic or insulating behavior (*5*). Calculations for Si nanowires

Department of Chemical Engineering and Texas Materials Institute, University of Texas, Austin, TX 78712, USA.

*To whom correspondence should be addressed. E-mail: korgel@mail.che.utexas.edu

†Present address: Department of Chemistry, University College Cork, Ireland.

have shown that bond orientational order will influence their physical properties as well (*6*). These effects, however, have not been experimentally observed in Si nanowires, largely because of inability to obtain highly crystalline samples with narrow wire diameter distributions and tunable crystallographic orientation.

The high-aspect-ratio quantum wires (those with a high ratio of length to diameter) must have diameters less than 10 nm. Self-assembly strategies are best suited for directing materials synthesis on this mesoscopic length scale. Many successful strategies have been developed for semiconductor quantum dots (*7*). These methods rely on the ability to isolate nanometer-scale reaction compartments, control crystallization kinetics, provide a growth template, or some combination of these. Strategies have also been developed for semiconductor nanowire self-assembly in solution and in the gas phase; however, greater control over the wire diameter distributions and crystallinity is desired (*1, 2, 8*). Certainly, the production of single-walled carbon nanotubes in the gas phase demonstrates that self-assembly methods can yield very high-quality one-dimensional (1D) materials (*2*). Because solution-phase synthetic methods can enable great chemical flexibility and synthetic tunability, as has been demonstrated for quantum dots (*7*), it is desirable to extend the highly controlled solution-phase self-assembly methods to semiconductor nanowires. The work presented here demonstrates the ability to self-assemble Si nanowires in solution with a very high degree of control, producing wires with highly crystalline cores, narrow diameter size distributions, aspect ratios greater than 1000, and tunable crystallographic orientation.

We used solvent-dispersed, size-monodisperse, alkanethiol-capped gold (Au) nanocrystals to direct Si nanowire growth with narrow wire diameter distributions. Sterically stabilized Au nanocrystals were dispersed in supercritical hexane with a silicon precursor, diphenylsilane, at temperatures of 500°C and 270 bar (or 200 bar in some cases). At these temperatures, the diphenylsilane decomposes to Si atoms. The phase diagram for Si and Au indicates that at temperatures above 363°C, Si and Au form an alloy in equilibrium with pure solid Si when the Si concentration with respect to Au is greater than 18.6% (*2*). Under the reaction conditions used, the Si atoms most likely dissolve into the sterically stabilized Au nanocrystals until reaching supersaturation, at which point they are expelled from the particle as a thin nanometer-scale wire. Figure 1 shows a schematic of the nanocrystal-directed nanowire self-assembly process. This fluid medium provides the high temperatures necessary to promote Si crystallization. More than 30 years ago, this phase behavior was exploited to grow micrometer-diameter Si wires on a substrate by chemical vapor deposition (*9*). Au droplets placed on a Si substrate directed Si "whisker" formation in the vertical direction by a process called vapor-liquid-solid (VLS) growth (*10*). Recently, VLS growth was applied to the gas phase to form nanometer-scale Si wires (*11*). Gas-phase liquid Au droplets were produced by laser ablation in the presence of silane at high temperatures. Si wires spontaneously formed. Although this method produces relatively large quantities of nanometer-scale Si wires, the liquid droplets naturally have a broad size distribution, and therefore, the nanowires also have relatively broad size distributions (*10*). In the supercritical (sc) fluid environment, relatively size-monodisperse Au nanocrystals can be maintained to seed nanowire growth at the high temperatures necessary to achieve wire growth.

Figure 2 shows typical transmission electron microscopy (TEM) images of the wires formed with this process. The 40 to 50 Å diameter nanowires are 1D "single crystals" with extremely narrow diameter size distributions (less than ±10% SD about the mean wire diameter) and aspect ratios greater than 1000. These nanowires photoluminesce in the blue because of quantum confinement effects (Fig. 3), and the optical properties were found to strongly depend on the wire crystallographic orientation measured by TEM and electron diffraction: <100> oriented wires exhibit higher exciton energies than the <110> oriented wires with a diameter of 40 to 50 Å.

The Si nanowires were prepared by thermally degrading diphenylsilane in sc-hexane [supercritical temperature and pressure (T_c = 235°C; P_c = 30 bar)] at 500°C and 200 or 270 bar in an inconnell high-pressure cell (*12*). The nanowire synthesis relies on dodecanethiol-capped Au nanocrystals, ranging between 20 and 30 Å in diameter, formed using standard arrested precip-

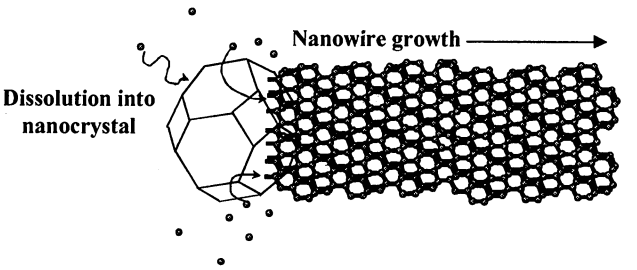

Fig. 1. Schematic of the proposed nanowire growth process. Thermal degradation of diphenylsilane results in free Si atoms that dissolve in the Au nanocrystal until reaching a Si:Au alloy supersaturation, when Si is expelled from the nanocrystal as a crystalline nanowire. This wire is depicted with a preferred <111> orientation.

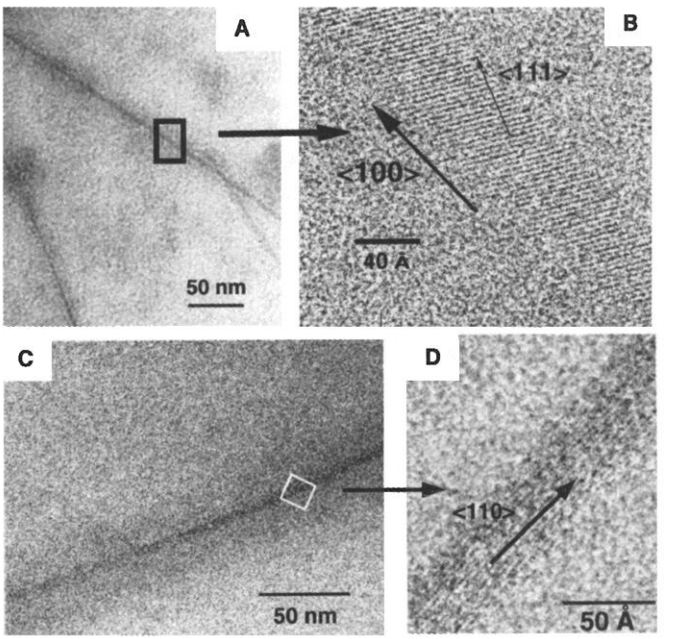

Fig. 2. TEM images of Si nanowires synthesized at 500°C in hexane at pressures of 200 bar (**A** and **B**) and 270 bar (**C** and **D**). The nanowires are highly crystalline. In both (B) and (D), the lattice fringes are the Si (111) planes, separated by 3.14 Å. The nanowire samples were prepared for imaging by dispersing them in chloroform and evaporating a drop onto a carbon-coated copper TEM grid. A JEOL 2010 transmission electron microscope with 1.7 Å point-to-point resolution operating with a 200-kV accelerating voltage with a GATAN digital photography system was used for TEM. In situ EDS (Oxford Instruments) confirmed that the samples were high in Si content with residual C and O.

itation procedures to direct wire formation (*13*). A light brown precipitate consisting of Si nanowires formed during the course of the reaction (TEM images in Fig. 2). No color change was observed in the absence of diphenylsilane. In the absence of Au nanocrystals, the solution quickly turned from orange to brown and then to clear as polydisperse black micrometer-sized Si particles formed and settled on the walls of the reaction vessel. Chloroform was used to extract the nanowires from the cell upon cooling and depressurization. The sc solvent provides a high diffusion coefficient, on the order of 10^{-3} to 10^{-4} cm^2 s^{-1} (*14*), which is necessary for rapid reactant diffusion to help avoid Si nanocrystal growth in the bulk solvent.

The Si nanowires were characterized with a variety of techniques. Energy dispersive x-ray spectroscopy (EDS) and x-ray photoelectron spectroscopy (XPS) revealed that the nanowires consisted of a high concentration of Si, with residual amounts of C, O, and Au (*15*). As shown in Fig. 2, TEM revealed Si (111) lattice planes with 3.14 Å spacing in all of the samples, confirming that the nanowire cores did indeed consist of pure crystalline Si. The wires exhibited diameters approximately 10 Å larger than the nanocrystal diameter, and the thickness appeared to fluctuate along the length of the wire by ±1 lattice plane; however, these variations may result from the resolution limitations of the microscope itself. The wires formed at 200 bar exhibited a preponderance of <100> oriented wires, whereas the samples synthesized at 270 bar contained wires oriented almost exclusively along the <110> direction. Pressure appears to be the determining factor in tuning the lattice orientation in the wire: At higher pressures, the brown color appeared sooner than at lower pressures, indicating that diphenylsilane degrades faster at higher pressures, and therefore it appears that the nanowire growth rate affects the nanowire orientation. A semitransparent coating of oxide or hydrocarbon on the nanowires was apparent in the TEM images of all of the wires (*15*). It is unclear whether this coating forms after removal from the reaction vessel or if it forms on the wire surface during nanowire growth. However, the thickness of this coating increased over time if the wires were exposed to air.

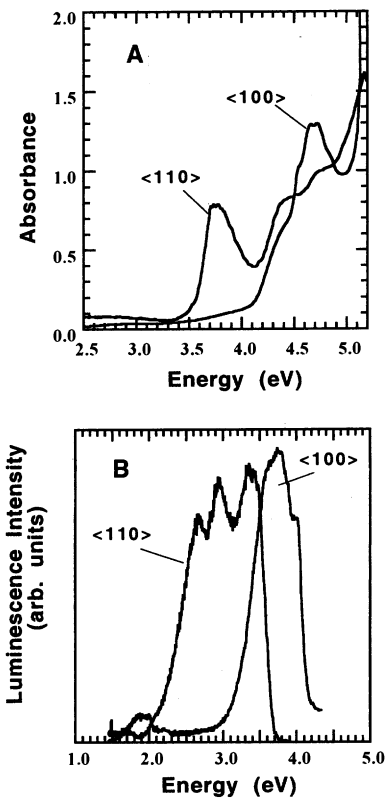

Fig. 3. Room-temperature optical properties of the Si nanowires imaged in Fig. 2. (**A**) Absorbance spectra (from a Varian Cary 500 UV-Vis-NIR spectrophotometer) for a dilute nanowire suspension in hexane. The spectra labeled <100> are for nanowires formed at 200 bar (Fig. 2, A and B) and <110> at 270 bar (Fig. 2, C and D). (**B**) Photoluminescence spectra (from a SPEX Fluorolog-3 spectrophotometer) of nanowires dispersed in hexane with excitation energies of 4.46 eV (277 nm, <100>) and 4.12 eV (300 nm, <110>).

The absorption edge of the Si nanowires was strongly blue-shifted from the bulk indirect band gap of 1.1 eV and showed sharp discrete absorbance features and relatively strong "band edge" photoluminescence (PL). These optical properties likely result from quantum confinement effects, although we cannot rule out the possibility of additional surface states as well (*2, 16*). The <110> oriented nanowires exhibited distinctly molecular-type transitions, whereas the <100> oriented wires exhibited a strong feature reminiscent of the L→L critical point in the Si band structure with a slowly rising phonon-assisted optical transition. The <100> oriented wires exhibited a significantly higher exciton energy than the <110> oriented wires, as predicted by Yorikawa and co-workers (*6*).

Thus, the tunability of the lattice orientation in the silicon nanowires leads to different optical properties that could be exploited in applications. The <100> nanowires exhibited a single sharp PL feature at 3.75 eV with a weak shoulder shifted to lower energy at 1.9 eV. The weak low-energy peak likely results from the surrounding oxide (*16*). The <110> oriented wires exhibited three distinct peaks at 3.35, 2.9, and 2.55 eV. The relatively robust PL exhibited initially after synthesis became completely quenched over the course of about 1 week, but the PL energy did not appear to shift to lower energy upon exposure to air. Certainly, the lattice orientation is expected to affect electron transport in future mesoscopic interconnects employing Si and must be considered in the design and manufacture of such devices.

References and Notes

1. For a recent review, see S. M. Prokes and K. L. Wang, *Mater. Res. Sci. Bull.* **24**, 13 (1999) and references therein.
2. J. Hu, T. W. Odom, C. M. Lieber, *Acc. Chem. Res.* **32**, 435 (1999).
3. Many calculations of quantum confinement in silicon nanowires exist. See, for example, F. Buda, J. Kohanoff, M. Parrinello, *Phys. Rev. Lett.* **69**, 1272 (1992); A. J. Read *et al.*, *Phys. Rev. Lett.* **69**, 1232 (1992); G. D. Sanders and Y.-C. Chang, *Phys. Rev. B* **45**, 9202 (1992); M.-Y. Shen and S.-L. Zhang, *Phys. Lett. A* **176**, 254 (1993); C.-Y. Yeh, S. B. Zhang, A. Zunger, *Phys. Rev. B* **50**, 14405 (1994); and references therein.
4. L. Brus, *J. Phys. Chem.* **98**, 3575 (1994).
5. J. W. Mintmire, B. I. Dunlap, C. T. White, *Phys. Rev. Lett.* **68**, 631 (1992); N. Hamada, S.-I. Sawada, A. Oshiyama, *Phys. Rev. Lett.* **68**, 1579 (1992).
6. H. Yorikawa, H. Uchida, S. Muramatsu, *J. Appl. Phys.* **79**, 3619 (1996).
7. A. P. Alivisatos, *Science* **271**, 933 (1996).
8. T. J. Trentler *et al.*, *Science* **270**, 1791 (1995); T. J. Trentler *et al.*, *J. Am. Chem. Soc.* **119**, 2172 (1997); J. R. Heath, *Chem. Phys. Lett.* **208**, 263 (1993).
9. R. S. Wagner and W. C. Ellis, *Appl. Phys. Lett.* **4**, 89 (1964).
10. For example, see J. Westwater, D. P. Gosain, S. Tomiya, S. Usui, H. Ruda, *J. Vac. Sci. Technol. B* **15**, 554 (1997) and references therein.
11. A. M. Morales and C. M. Lieber, *Science* **279**, 208 (1998); Y. F. Zhang *et al.*, *Appl. Phys. Lett.* **72**, 1835 (1998).
12. Under a nitrogen atmosphere, the nanocrystals were dispersed in diphenylsilane with a Au:Si mole ratio of 0.1%, then loaded into an inconnell high-pressure cell (0.2 ml) and sealed under a nitrogen atmosphere. The cell was attached, via a three-way valve, to a stainless steel high-pressure tube (~40 cm^3) equipped with a stainless steel piston. A high-pressure liquid chromatography pump (LDC Analytical) was used to pump deionized water into the back of the piston and displace oxygen-free anhydrous hexane through an inlet heat exchanger and into the reaction cell to the desired pressure of either 200 or 270 bar. The cell was covered with heating tape (0.6 m) and heated to 500°C (±0.2 °C) using a platinum resistance thermometer and a temperature controller. The reaction proceeded at these conditions for 1 hour.
13. The dodecanethiol-capped Au nanocrystals were formed using the procedures outlined in M. Brust, M. Walker, D. Bethell, D. J. Schiffrin, R. Whyman, *J. Chem. Soc. Chem. Commun.* **1994**, 801 (1994); B. A. Korgel and D. Fitzmaurice, *Phys. Rev. Lett.* **80**, 3531 (1998). The nanocrystals had a mean diameter of 25 Å with a SD about the mean of ±20%.
14. M. A. McHugh and V. J. Krukonis, *Supercritical Fluids Extraction: Principles and Practice* (Butterworth-Heinman, MA, ed. 2, 1993).
15. XPS revealed that the samples consisted of less than 0.1% Au, with ratios of Si:O of 2:1 and Si:C of 1:3. The relatively high concentrations of carbon and oxygen stem from the fact that the volume of the ~40 Å thick coating of carbon and oxygen surrounding the 40 Å diameter wire has a volume three times that of the silicon core.
16. M. V. Wolkin, J. Jorne, P. M. Fauchet, G. Allan, C. Delerue, *Phys. Rev. Lett.* **82**, 197 (1999).

17. K.P.J. thanks the U.S. Department of Energy and NSF for support. B.A.K. thanks DuPont for support through a Young Professor Grant.

22 October 1999; accepted 28 December 1999